

Synthesis and electrochemical performance of La_2CuO_4 as a promising coating material for high voltage Li-rich layered oxide cathodes

Fuliang Guo(郭福亮), Jiaze Lu(卢嘉泽), Meihua Su(苏美华), Yue Chen(陈约), Jieyun Zheng(郑杰允), Liang Yin(尹良), and Hong Li(李泓)

Citation: Chin. Phys. B, 2023, 32 (**8**): 088201. DOI: 10.1088/1674-1056/acd2bc
Journal homepage: http://cpb.iphy.ac.cn; http://iopscience.iop.org/cpb

What follows is a list of articles you may be interested in

Electron density distribution of $LiMn_2O_4$ cathode investigated by synchrotron powder x-ray diffraction

Tongtong Shang(尚彤彤), Dongdong Xiao(肖东东), Qinghua Zhang(张庆华), Xuefeng Wang(王雪锋), Dong Su(苏东), and Lin Gu(谷林)

Chin. Phys. B, 2021, 30 (**7**): 078202. DOI: 10.1088/1674-1056/abf347

Computational screening of doping schemes for $LiTi_2(PO_4)_3$ as cathode coating materials

Yu-Qi Wang(王宇琦), Xiao-Rui Sun(孙晓瑞), Rui-Juan Xiao(肖睿娟), Li-Quan Chen(陈立泉)

Chin. Phys. B, 2020, 29 (**3**): 038202. DOI: 10.1088/1674-1056/ab7186

Influence of carbon coating on the electrochemical performance of SiO@C/graphite composite anode materials

Hao Lu(陆浩), Junyang Wang(汪君洋), Bonan Liu(刘柏男), Geng Chu(褚赓), Ge Zhou(周格), Fei Luo(罗飞), Jieyun Zheng(郑杰允), Xiqian Yu(禹习谦), Hong Li(李泓)

Chin. Phys. B, 2019, 28 (**6**): 068201. DOI: 10.1088/1674-1056/28/6/068201

Conductivity and applications of Li-biphenyl-1, 2-dimethoxyethane solution for lithium ion batteries

Geng Chu(褚赓), Bo-Nan Liu(刘柏男), Fei Luo(罗飞), Wen-Jun Li(李文俊), Hao Lu(陆浩), Li-Quan Chen(陈立泉), Hong Li(李泓)

Chin. Phys. B, 2017, 26 (**7**): 078201. DOI: 10.1088/1674-1056/26/7/078201

Structural and magnetic properties of $LiNi_{0.5}Mn_{1.5}O_4$ and $LiNi_{0.5}Mn_{1.5}O_{4-\delta}$ spinels: A first-principles study

Xin Xiao-Gui (忻晓桂), Shen Jing-Qin (沈静琴), Shi Si-Qi (施思齐)

Chin. Phys. B, 2012, 21 (**12**): 128202. DOI: 10.1088/1674-1056/21/12/128202

RAPID COMMUNICATION

Synthesis and electrochemical performance of La_2CuO_4 as a promising coating material for high voltage Li-rich layered oxide cathodes

Fuliang Guo(郭福亮)[1,2], Jiaze Lu(卢嘉泽)[1], Meihua Su(苏美华)[3], Yue Chen(陈约)[1], Jieyun Zheng(郑杰允)[1], Liang Yin(尹良)[1,4,†], and Hong Li(李泓)[1,2,3,4,‡]

[1] *Beijing Advanced Innovation Center for Materials Genome Engineering, Key Laboratory for Renewable Energy, Beijing Key Laboratory for New Energy Materials and Devices, Institute of Physics, Chinese Academy of Sciences, Beijing* 100190, *China*

[2] *School of Physical Sciences, University of Chinese Academy of Sciences, Beijing* 100049, *China*

[3] *Tianmu Lake Institute of Advanced Energy Storage Technologies, Liyang* 213300, *China*

[4] *Yangtze River Delta Physics Research Center, Liyang* 213300, *China*

(Received 11 February 2023; revised manuscript received 24 April 2023; accepted manuscript online 5 May 2023)

The structural transformations, oxygen releasing and side reactions with electrolytes on the surface are considered as the main causes of the performance degradation of Li-rich layered oxides (LROs) cathodes in Li-ion batteries. Thus, stabilizing the surfaces of LROs is the key to realize their practical application in high energy density Li-ion batteries. Surface coating is regarded as one of the most effective strategies for high voltage cathodes. The ideal coating materials should prevent cathodes from electrolyte corrosion and possess both electronic and Li-ionic conductivities simultaneously. However, commonly reported coating materials are unable to balance these functions well. Herein, a new type of coating material, La_2CuO_4 was introduced to mitigate the surface issues of LROs for the first time, due to its superb electronic conductivity (26–35 mS·cm^{-1}) and lithium-ionic diffusion coefficient (10^{-12}–10^{-13} cm^2·s^{-1}). After coating with the La_2CuO_4, the capacity retention of $Li_{1.2}Ni_{0.54}Co_{0.13}Mn_{0.13}O_2$ cathode was increased to 85.9% (compared to 79.3% of uncoated cathode) after 150 cycles in the voltage range of 2.0–4.8 V. In addition, only negligible degradations on the deliverable capacity and rate capability were observed.

Keywords: La_2CuO_4, electronic conductivity, Li-ionic conductivity, Li-rich layered oxides, high voltage

PACS: 82.47.Aa, 82.45.Fk **DOI:** 10.1088/1674-1056/acd2bc

1. Introduction

Li-rich layered oxides (LROs) have been considered as one of the most critical cathode materials for the next-generation Li-ion battery due to their high gravity energy density and low cost.[1–3] It is well known that it can deliver capacity as high as 250–400 mA/g when charged to 4.8 V or even higher.[2,4] However, its practical application is hindered by several issues, such as low initial Coulombic efficiency, poor rate capability, cycling stability, voltage fading and so on.[5–9] These unsatisfied electrochemical properties are related to oxygen redox activities, cation migrations and interfacial side reactions, especially when charged to high voltages.[10–13] To address these limitations, various modification strategies were applied, such as composition regulation, synthetic method control, element doping, surface coating and surface chemical treatment.[14] Among them, the surface coating has been proved to be an effective way to mitigate surface issues by inhibiting the electrolyte corrosion and transition metal ion dissolution.[15]

Numerous coating materials have been applied to protect the surfaces of LROs, such as fluorides (e.g., AlF_3, CaF_2, FeF_3, CeF_3 and LiF), metallic oxides (e.g., Al_2O_3, MnO_2, SnO_2, V_2O_5, CeO_2 and MoO_3) , phosphates (e.g., Li_3PO_4, $AlPO_4$, $CePO_4$, $FePO_4$, $LiFePO_4$ and LATP), ionic conductors (e.g., $LiNi_{0.5}Mn_{1.5}O_2$, $Li_4Ti_5O_{12}$ and $LiNbO_3$) and polymers (e.g., PEDOT, dopamine, conducting polypyrrole and PAN).[15] Although these coating materials were able to stabilize the surface structure and suppress interfacial side reactions of LROs, their limited electronic or ionic conductivity has negative effects on the rate capabilities or deliverable capacities in many cases.

Herein, La_2CuO_4,[16–19] a room temperature superconductor, was utilized as a new type of coating materials for the first time, due to its excellent electronic and ionic conductivities as reported.[20] More importantly, it has been verified that La_2CuO_4 is capable of absorbing oxygen through a reversible redox reaction ($La_2CuO_4 + xO_2/O^- \rightarrow La_2CuO_{4+x}$) at room temperature, in which O_2 or O^- is captured along with the oxidation of Cu^{2+} into Cu^{3+}.[16,21–25] Considering the universal issue of oxygen releasing in oxide cathodes at high voltage, such a unique property of La_2CuO_4 could be utilized to store oxygens produced by cathode materials during charge process

†Corresponding author. E-mail: lyin@iphy.ac.cn
‡Corresponding author. E-mail: hli@iphy.ac.cn

© 2023 Chinese Physical Society and IOP Publishing Ltd

and return them back to the cathodes during discharge process reversibly. Therefore, La_2CuO_4 is a promising coating material for cathode materials that are suffering from severe oxygen releasing when operated at high voltage.

The present work aims to screen the synthesis conditions of La_2CuO_4 materials and evaluate its electrochemical performances in Li-ion batteries systematically. To demonstrate the coating capability of La_2CuO_4, nano-sized La_2CuO_4 coated LROs powders were prepared. Experiments reveal that La_2CuO_4 coated LROs exhibit better cycling life while remaining the rate performance in the voltage range of 2.0–4.8 V.

2. Experiment

2.1. Materials synthesis

The La_2CuO_4 powder was prepared by solid state reactions based on the previous reported method.[26] $C_6H_9LaO_6{\cdot}1.5H_2O$ (Aladdin, 99.99%) and $C_4H_6CuO_4{\cdot}H_2O$ (Aladdin, 99.95%) precursors were mixed thoroughly in a molar ratio of 2:1 by the mortar and pestle. The mixture was heated at temperatures varying from 400 °C to 1000 °C for 12 hours in air. To prepare the La_2CuO_4 coated LROs, the 4.5 wt.% nano-sized La_2CuO_4 aqueous slurry (Huzhou Namu Nanotechnology Co.) was mixed with $Li_{1.2}Ni_{0.54}Co_{0.13}Mn_{0.13}O_2$ powders (Tianmu Lake Institute of Advanced Energy Storage Technologies) homogeneously. After drying the mixture at 60 °C in a vacuum oven for 12 hours, the powders was ground thoroughly and heated at 800 °C for 12 hours in air.

2.2. Materials characterization

The morphologies of the as-prepared La_2CuO_4 samples and the La_2CuO_4 coated LROs were characterized by the field emission scanning electron microscope (FE-SEM, S4800, Hitachi) with energy dispersive spectrometer (EDS). The lab x-ray powder diffraction (XRD) data were collected in a 2θ range of 10°–70° with an increment of 0.05° on the Bruker D8 Advance (Cu radiation). The electronic conductivity of La_2CuO_4 was measured by four-point probe RTS-5 (Four Probe Tech Ltd.). 0.1 g powder was placed into a 15 mm diameter cylinder mold and pressed into a disk at the pressure of 12 kN and then the electronic conductivity of the pellet was measured. For each sample, six pellets were prepared and measured to insure the accuracy. The x-ray photoelectron spectroscopy (XPS) data were collected on an ESCALAB 250 Xi (Thermo Fisher) with a monochromatic 150-W Al Ka radiation. The XPS data were analyzed with the Thermo Advantage and the binding energies were calibrated by the C 1s line at 284.8 eV. The element contents of the samples were measured by inductively coupled plasma optical emission spectrometry ICP-OES (iCAP 7000, Thermo Fisher). Electron diffraction pattern (TEM) was obtained from transmission electron microscopy (JEM F-200, JEOL).

2.3. Electrochemical measurements

The working electrodes were prepared by casting the mixture of La_2CuO_4 material 80.0 wt.%, super P 10.0 wt.%, and polytetrafluoroethylene (PVDF) 10.0 wt.% dissolved with N-methyl pyrrolidone (NMP) solvent onto Ti foil. The electrodes were punched into 12 mm disks and then dried at 120 °C in a vacuum oven for 12 hours. The loading of active materials on these cathode films is ~ 3 mg/cm^2. For La_2CuO_4 coated LROs, the working electrodes were prepared in the same procedure, except that Ti foil was replaced by Al foil.

The electrochemical performances were tested using CR2032 coin cells, assembled in an Ar-filled glove box. 1 M $LiPF_6$ in fluoroethylene carbonate (FEC) and dimethyl carbonate (EMC) (2:8 by volume) were used as electrolytes. The lithium foil (500 μm thickness) was used as the counter electrode and the polyethylene (25 μm thickness) was used as the separator. The cycling of the as-prepared coin cells was carried out on the Land CT3001A battery test system (Land, Wuhan, China). Cyclic voltammetry tests were performed on the CHI 600 (Chinstruments, Shanghai, China). The electrochemical impedance spectroscopy (EIS) of the coin cells was performed on the Zahner pro impedance analyzer (Zahner, Germany) at open circuit voltage with a 10 mV amplitude within the frequency range of 5 MHz–50 MHz.

3. Results and discussion

3.1. Physical and electrochemical properties of La_2CuO_4

An overlay of the XRD patterns of La_2CuO_4 samples synthesized at various temperatures is shown in Fig. 1. Ideal La_2CuO_4 phase can be indexed to $I4/mmm$.[27] The appearance of La_2CuO_4 reflections can be well identified in the pattern of the sample synthesized at 600 °C (Fig. 1(c)), accompanying with several impurities, which are CuO, La_2O_3, La_2CO_5 and $La_8Cu_7O_{19}$. A well crystallized La_2CuO_4 phase is formed at 700 °C (Fig. 1(d)). Increasing the sintering temperature step by step to 1000 °C does not affect the purity of the La_2CuO_4 phase. The higher the temperature, the sharper the diffraction peaks, which indicates increased crystallinities. However, the morphologies of these samples are quite different as shown in Fig. 2. The particles of La_2CuO_4–700 °C are porous and fluffier with size distribution of 5–20 μm. Much smaller and denser secondary particles are formed as the sintering temperature increases. A transition of secondary particle from porous polycrystalline to large single-crystal is observed clearly when the temperature is elevated from 900 °C to 1000 °C (Figs. 2(c)–2(d)). It is known that large single-crystal is helpful to reduce the specific surface area of ma-

terials, thus reducing the interphase resistance between electrolytes. To verify the ratio of La/Cu, ICP-OES was performed. Table S1 shows that the La/Cu ratio has some deviations compared with the designed value which is supposed to be affected by the crystal water of reagents. TEM images reveal the lattice fringes of La_2CuO_4–1000 °C that can refer to the K_2NiF_4 structure ($I4/mmm$). The interplanar spacing of the lattice planes is measured to be 0.287 nm which is well indexed to the (113) fringes as shown in Fig. S1.

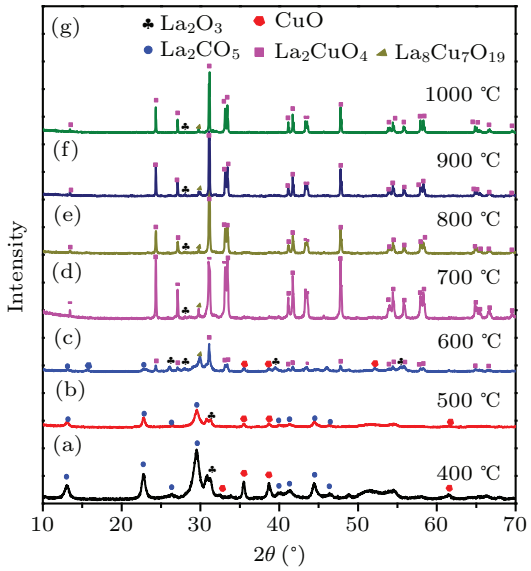


Fig. 1. XRD patterns of La_2CuO_4 synthesized at (a) 400 °C, (b) 500 °C, (c) 600 °C, (d) 700 °C, (e) 800 °C, (f) 900 °C, and (g) 1000 °C.

The surface chemical status of La_2CuO_4 samples was measured by XPS as shown in Fig. 3. The C 1s spectrum displays the typical peaks which locate at 284.8 eV and 289.0 eV ascribed to C–C and C=O, respectively and it is likely to reflect carbon and carbonates residues resulting from H_2O and CO_2 in the air on the surface. Figure 3(b) shows the O 1s spectrum. A shoulder peak around 298.5 eV beside a main peak 531.0 eV is found, which is assigned to the oxygens adjacent to lanthanum and the oxygens in the Cu–O plane.[28] The binding energies of La $3d_{5/2}$ and La $3d_{3/2}$ are 834.3 eV/837.7 eV and 850.8 eV/854.5 eV with a separation of about 3.5 eV, agreed with the literature.[29] Figure 3(d) shows two main peaks and two satellites in Cu 2p spectrum and the binding energies of 933.00 eV and 952.35 eV are corresponding to Cu $2p_{3/2}$ orbital and Cu $2p_{1/2}$ orbital, respectively. Satellite peaks of Cu (II) appear at the positions of binding energies of 941.68 eV and 961.23 eV, corresponding to Cu $2p_{3/2}$ orbital and Cu $2p_{1/2}$ orbital, respectively.[28]

The electronic conductivities of La_2CuO_4 samples vary from 27 mS/cm to 34 mS/cm, as shown in Fig. 4, which are much higher than those of common layered oxide cathodes.[30–32] Interestingly, the electronic conductivity is sensitive to the sintering temperature and the correlation is not simply linear. The La_2CuO_4 sample obtained at 800 °C achieves the maximum electronic conductivity and its color is darker. It is possible due to the change of morphology as nano single-crystal La_2CuO_4 promotes the press density of La_2CuO_4 disks. While fluffy morphology or large single-crystal is unfavorable to enhance the press density and the contacts between particles of disks are poor.

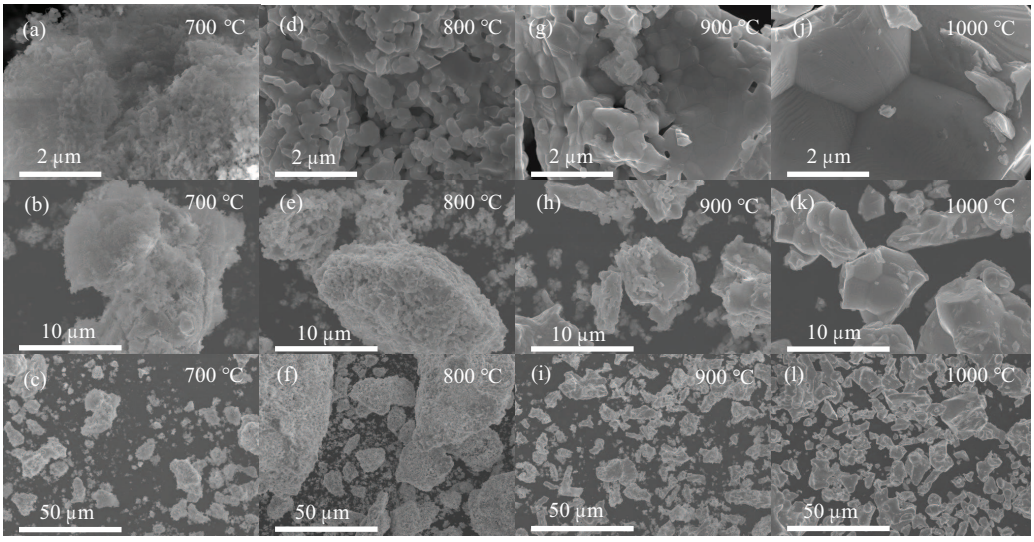


Fig. 2. SEM images of La_2CuO_4 synthesized at (a)–(c) 700 °C, (d)–(f) 800 °C, (e)–(h) 900 °C, and (j)–(l) 1000 °C.

To evaluate the electrochemical performance of La_2CuO_4 in Li-ion batteries, the cyclic voltammetry (CV) was conducted in voltage intervals of 0.005–2.0 V and 2.0–5.0 V. As shown in Figs. 5(a)–5(d), all samples present two reduction peaks. The peak around 0.005 V is sharp in the initial cycle but becomes mellow in the following two cycles. Another remarkable reduction peak appears at ∼ 1.0–1.1 V and the intensity is much weaker than the former one. Moreover, the peak located at ∼ 1.0–1.1 V disappears in the following cycles, which reveals that amounts of the Li-ions are trapped in

the electrode and result in irreversible loss. As the sintering temperature elevates, the irreversible peak becomes stronger, which indicates the loss of Li-ions. Two reversible oxidation peaks are observed in the voltage intervals of 0.005–2.0 V. They are located at 0.17 V and 0.95 V and the peak intensities also increase with sintering temperature increase owing to the probably improved ion diffusion. The cyclic voltammetry curves of La_2CuO_4 conducted in the voltage intervals of 0.005–2.0 V are extremely similar to those of lithium intercalation compounds, such as graphite and hard carbon.[33–35] Thus, it is believed that the lithiation–delithiation mechanism may be similar. Since no lithium content presents in the pristine samples, the reversible redox peaks shown in Figs. 5(e)–5(h) reflect the redox reaction of La_2CuO_4 itself. The oxidation peak at 4.5-4.6 V (vs. Li^+/Li) may correspond to the oxygen involved reaction ($Cu^{2+}+O_2/O^- \rightarrow Cu^{3+}+O^{2-}$) and the reversible reduction at voltage of 3.0 V (vs. Li^+/Li) according to literatures.[16,21–25] The oxidation peak in the first cycle is stronger than the following cycles, indicating that most oxygen species in the electrolyte are absorbed in the initial charge.[25] However, the oxidation peak intensity decreases as the sintering temperature elevates. It is possible because the interphase reactions become wilder as the morphology of the samples is changed.

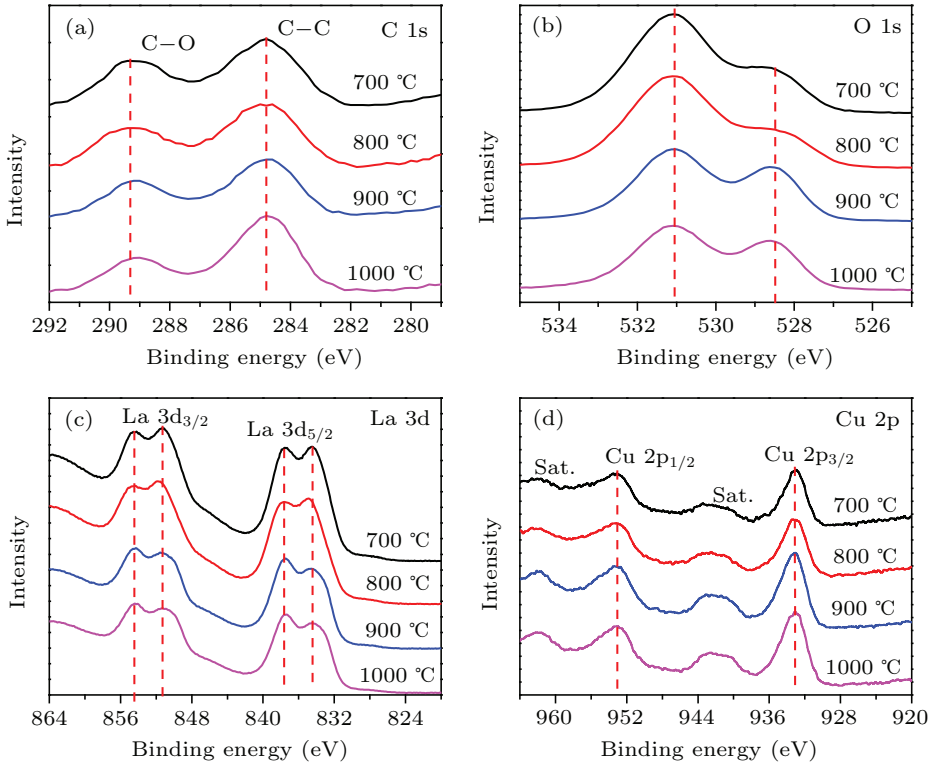


Fig. 3. XPS spectra of La_2CuO_4 samples, (a) C 1s, (b) O 1s, (c) La 3d and (d) Cu 2p.

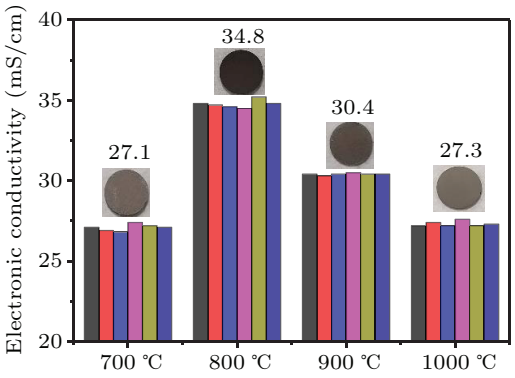


Fig. 4. The electronic conductivities of La_2CuO_4 disks. Six color bars of each sample represent six parallel disks.

To understand the structural revolution during the lithium intercalation process, a series of samples extracted from batteries at different SOCs were tested by XRD, as shown in Fig. 6(a). The open-circuit voltage (OCV) of the pristine coin cell is ∼ 3.0 V. After discharge the cell to 1.0 V, no obvious changes in the pattern are observed. However, most reflections of the La_2CuO_4 phase disappear as the voltage discharges to 0.005 V further. Surprisingly, all of these reflections reappear when the cell is charged back to 1.0 V again. The peak intensities become stronger as the voltage gradually increases to 5.0 V. Figure 6(b) presents the structural revolution after oxidation as the pristine sample is charged to 5.0 V directly. The diffraction patterns resemble closely though the oxidation reaction occurred around 4.5–4.6 V (vs. Li^+/Li). These excellent matching of peak positions and peak intensities before and after charge and discharge indicates the excellent reversibility of La_2CuO_4 lattice against Li-ion intercalation and its high structural stability at high voltage.

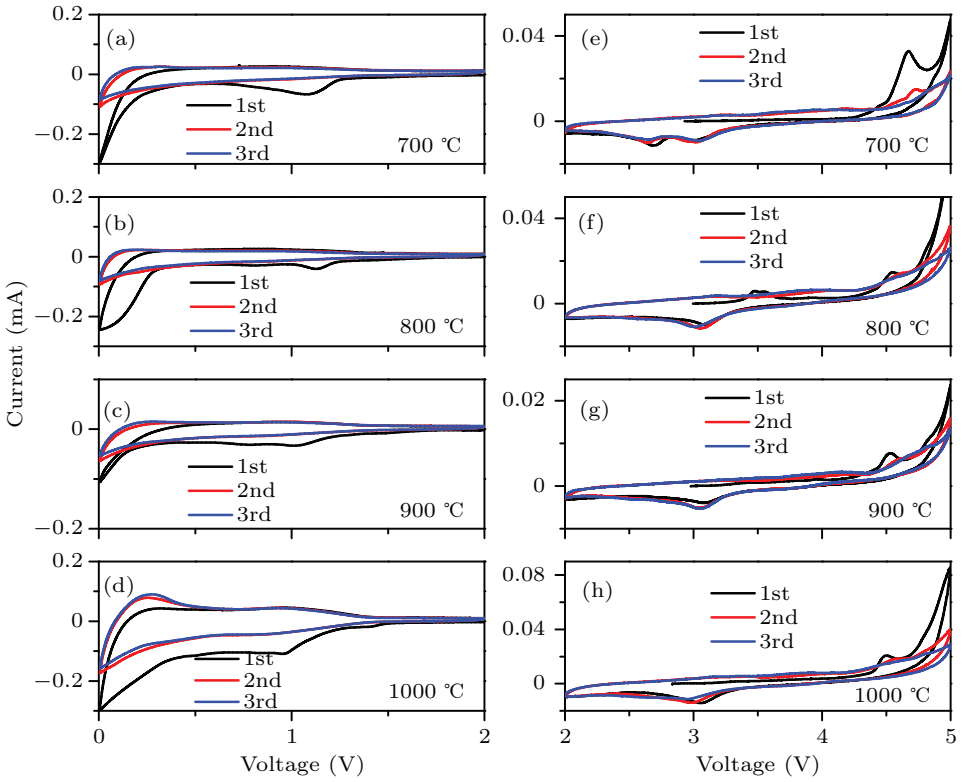


Fig. 5. Cyclic voltammetry curves of La_2CuO_4 synthesized at 700 °C, 800 °C, 900 °C and 1000 °C, (a)–(d) cycled in voltage intervals of 0.005–2.0 V and (c)–(h) cycled in voltage intervals of 2.0–5.0 V.

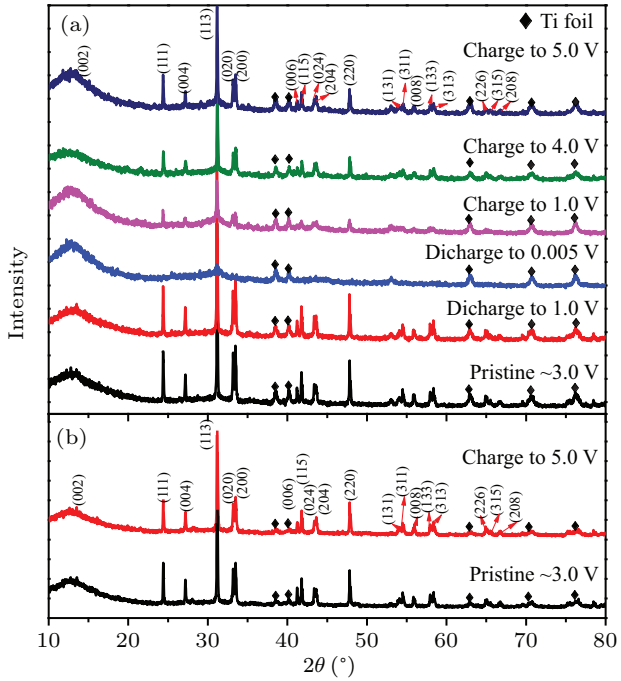


Fig. 6. XRD patterns of La_2CuO_4 samples at various SOCs, (a) structure revolutions during charging and discharging, and (b) a comparison of La_2CuO_4 patterns before and after cycling.

Figure 7 displays the electrochemical impedance spectroscopy of La_2CuO_4 in different lithiation and oxidation states. The impedance decreases as the voltage discharges to 0.15 V gradually and then increases at 0.005 V. This phenomenon is similar to that of graphite that the electrode polarization potential decreases as lithium ions intercalate into the active materials resulting in great change of charge transfer reactions while the impedance increases due to the SEI film becoming thicker and charge transfer resistance enlarged by the repulsion of the intercalated lithium ion at 0.005 V.[36] Moreover, the impedance is much lower as the sample sintering temperature is elevated to 1000 °C. It can be understood from the microstructure evolution of La_2CuO_4 that fluffier morphology is harmful. The impedance spectroscopy of the oxidation state presents a similar tendency as the lithiation process does which also indicates that the interphase condition was improved as the sintering temperature elevated.

To further identify the lithiated and delithiated reaction kinetics of La_2CuO_4, the lithium ion diffusion coefficient is calculated based on cyclic voltammetry measurement at 25 °C. Notably, two small oxidation peaks at 0.17 V and 0.95 V (vs. Li/Li^+) can be observed in Fig. 8(a), corresponding to the delithiation reactions. The peaks shift positively as scan rates ranging from 0.1 $mV{\cdot}s^{-1}$ to 0.4 $mV{\cdot}s^{-1}$. However, no obvious peaks are observed in the lithiation process which indicates no step-by-step lithiation existed during discharge. The anodic current peaks follow a linear relationship with the square root of scan rates, and the slope ($I_p/v^{0.5}$) of each reaction is calculated as shown in Fig. 8(b). Then, the lithium-ion diffusion coefficient D_{Li}^{+} for La_2CuO_4 sintering at 1000 °C is calculated based on the classical Randles–Sevcik equation[37]

$$I_{\rm p} = \left(2.69\times10^{5}\right)n^{1.5}SD_{\rm Li^+}^{0.5}C_{\rm Li}v^{0.5}, \quad (1)$$

where $I_{\rm p}$, n, S, $D_{\rm Li}^{+}$, $C_{\rm Li}$, and v denote the peak current, the charge transfer number, the surface area of active material, the lithium-ion diffusion coefficient and the concentration of lithium-ion in the cathode, respectively. Overall, the the lithium-ion diffusion coefficient is 10^{-12}–10^{-13} cm^2·s^{-1}, which is close to that of the layer oxide cathode.[30–32]

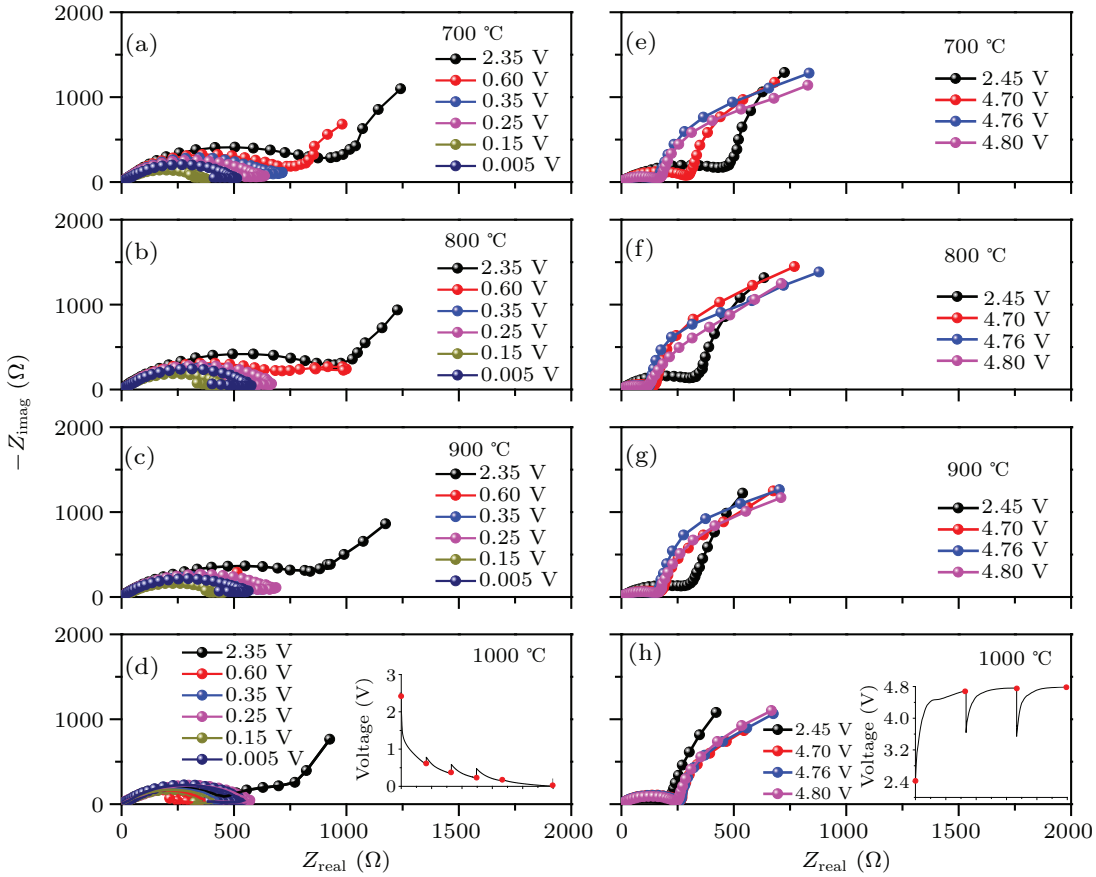


Fig. 7. Electrochemical impedance spectrum of La_2CuO_4, (a)–(d) impedance at different lithiation states (pristine cell discharged to 0.005 V gradually), and (e)–(h) impedance at different oxidation states (pristine cell charge to 4.8 V gradually).

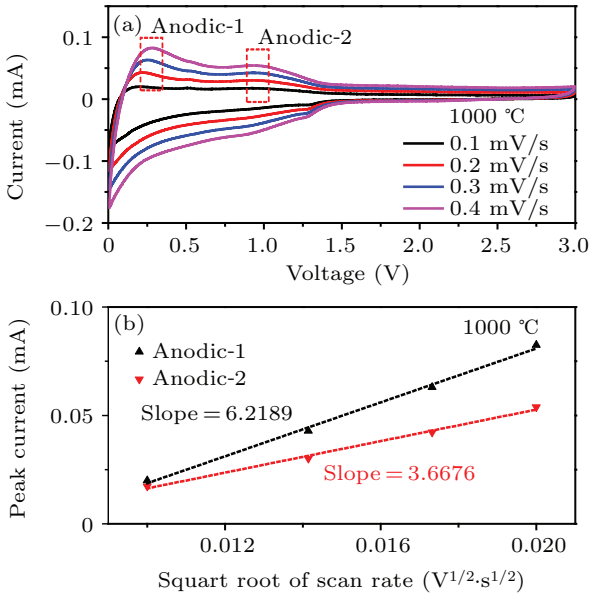


Fig. 8. Reaction kinetics of La_2CuO_4, (a) CV curves of La_2CuO_4 at different scan rates from 0.1 mV·s^{-1} to 0.4 mV·s^{-1}, and (b) plots of CV peak current of anodic oxidation processes versus the square root of the scan rates.

Since La_2CuO_4 possess both electronic and lithium-ion conductivities, it is worthy to investigate the cycle and rate performance as La_2CuO_4 can be battery material. Figure 9 reveals that the capacity of La_2CuO_4 is low, ranging from 26 mAh/g to 34 mAh/g at 0.1 C at room temperature and the initial Coulombic efficiency is only 30%–38% which indicate amounts of lithium ions are trapped as demonstrated by Fig. 5. However, the rate performance is not so poor, 61% capacity retention remains as the current density increases to 1.0 C, and the performance of the sample sintering at 1000 °C is better. The charge and discharge curves at different current rates are presented in Fig. S2. The cycle performance shows an inconceivable result that the capacity degrades in the first 40 cycles, and then gradually increases. After 200 cycles, the capacity is 1.2 times of that of the initial cycle. The abnormal growth of capacity which is not found in other intercalation compounds may result from the activation of Cu^{2+}/Cu^{3+} at high voltage, thus more lithium ions trapped in the initial discharge can be released from the stumble sites.[21]

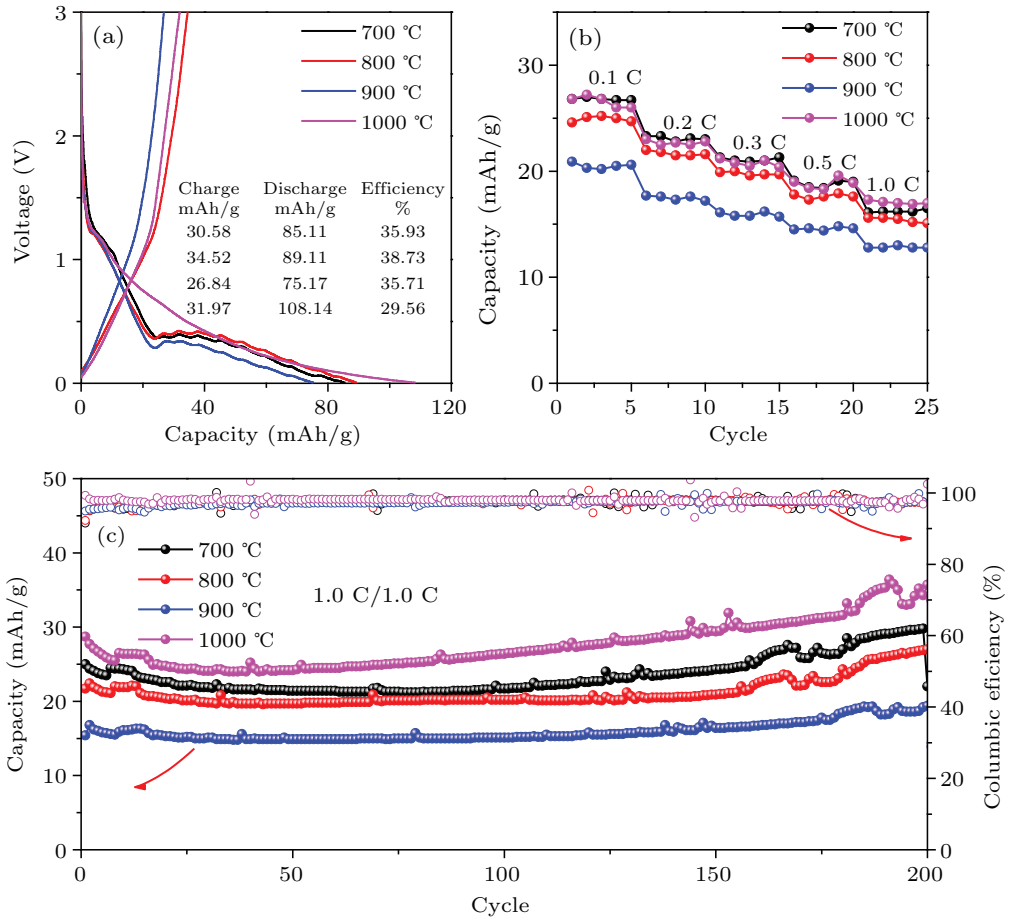


Fig. 9. Electrochemical performance of La_2CuO_4, (a) initial charge–discharge curves, (b) rate performance, and (c) cycle performance at a C-rate of 1.0 C/1.0 C in the voltage range of 2.0–4.8 V.

To sum up, La_2CuO_4 demonstrates superb electronic and lithium-ion conductivities, and the interphase between electrolytes is quite stable even though the voltage is charged to 4.8 V (vs. Li/Li^+), revealing its great potential as a coating material for high voltage cathodes.

3.2. Physical and electrochemical properties of La_2CuO_4 coated Li-rich layered oxide

To evaluate the performance of La_2CuO_4 as coating materials, 1 wt.% La_2CuO_4 was coated on the surface of $Li_{1.2}Ni_{0.54}Co_{0.13}Mn_{0.13}O_2$ using the method mentioned above. Figure 10 presents the morphologies of bare and coated LROs samples. The surface of the bare sample is smooth and clean. In contrast, a bunch of small particles with a size ranging from 60–400 nm are observed on the surface of the coated sample. These small particles are distributed on the cathode surface homogeneously, which is further confirmed by the elemental EDS mapping shown in Figs. 10(c)–10(i).

Electrochemical performance was investigated as shown in Fig. 11. The initial discharge capacity of the samples is very close (271 mA/g vs. 273 mA/g) at 0.1 C/0.1 C 2.0–4.8 V and the Coulombic efficiency is promoted from 80.71% to 85.59% after coating, which demonstrates that some side reactions are inhibited during formation. Moreover, the coated sample exhibits much better rate performance (138 mA/g vs. 118 mA/g) at high current density, the charge and discharge curves are shown in Fig. S3. Figure 11(c) shows the cycle performance of bare and LROs at 1.0 C in the voltage range of 2.0–4.8 V. The first cycle discharge capacity of the coated sample is 220 mAh/g, slightly higher than the bare one (213 mAh/g). After 150 cycles, the capacity decreases to 189 mAh/g and 174 mAh/g, respectively. Thus, the cycle performance is also improved after coating of La_2CuO_4.

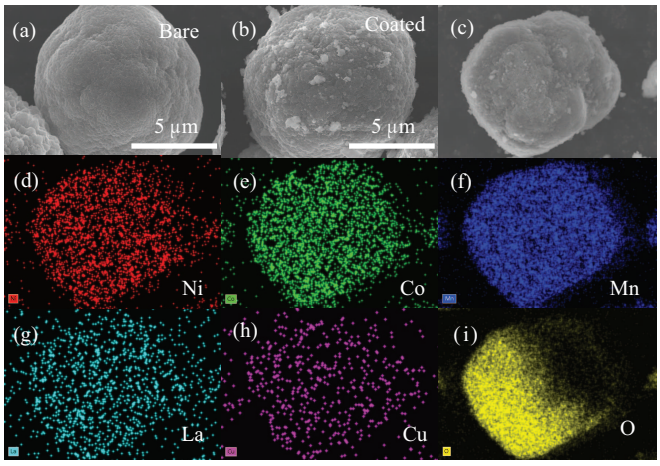


Fig. 10. (a) SEM images of bare LROs, (b) SEM images of La_2CuO_4 coated LROs, and (c)–(i) EDS mapping of La_2CuO_4 coated LROs.

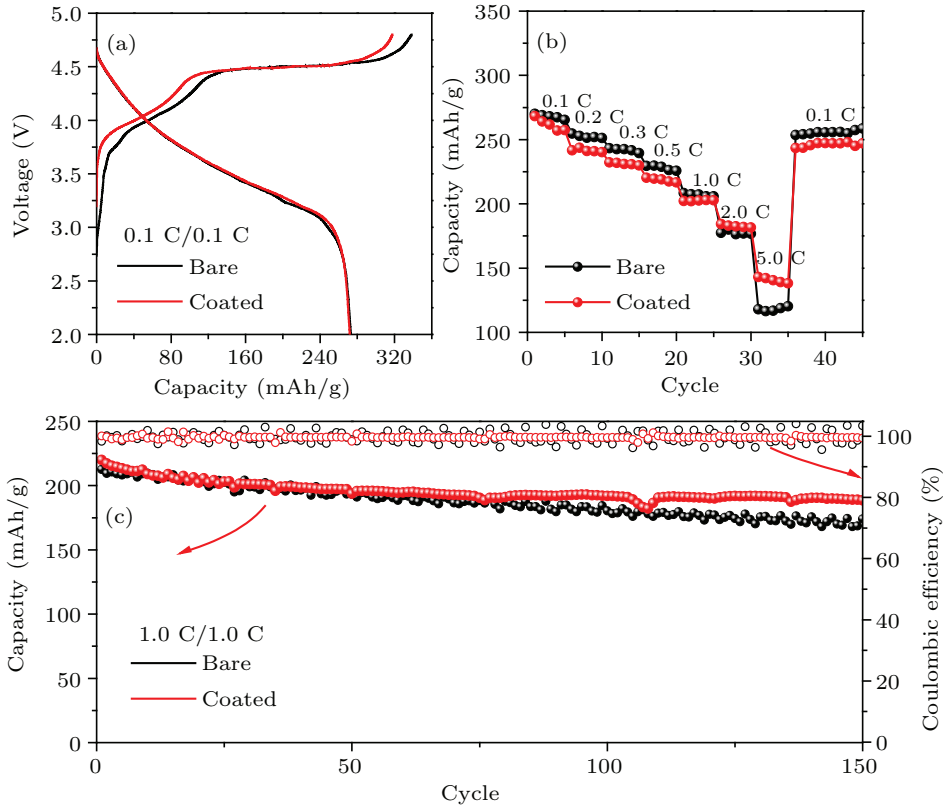


Fig. 11. Electrochemical performances of bare and La_2CuO_4 coated LROs, (a) the charge–discharge curve of the first cycle, (b) rate performance, and (c) cycle performance at 1.0 C/1.0 C in the voltage range of 2.0–4.8 V.

4. Conclusion and perspectives

In summary, a new coating material La_2CuO_4 was synthesized and its electrochemical performances were measured systematically. The coating material presents both superb electronic and lithium-ion conductivities and reacts mildly with electrolyte at high voltage. Therefore, nano La_2CuO_4 was coated on the surface of LROs. Preliminary experiments verified that the capacity retention of La_2CuO_4 coated LROs was improved to 85.9% (189 mA/g) after 150 cycles at 1.0 C/1.0 C in the voltage range of 2.0–4.8 V, which was higher than that of the bare material (79.3%, 174 mAh/g) and the rate performance was also promoted. This work highlights that La_2CuO_4 may be a promising candidate as coating material for the next-generation high energy density cathode materials and the treating parameter is very important for the coating process. Therefore, more studies are worthy to carry out and results will be displayed in our future works.

Acknowledgements

Project supported by the National Key Research and Development Program of China (Grant No. 2019YFE0100200), the National Natural Science Foundation of China (Grant No. U1964205), and the Beijing Municipal Science and Technology Commission (Grant No. Z191100004719001).

References

[1] Lu Z, MacNeil D and Dahn J 2001 *Electrochem. Solid-State Lett.* **4** A191
[2] Thackeray M M, Johnson C S, Vaughey J T, Li N and Hackney S A 2005 *J. Mater. Chem.* **15** 2257
[3] Schmuch R, Wagner R, Hörpel G, Placke T and Winter M 2018 *Nat. Energy* **3** 267
[4] Zuo Y, Li B, Jiang N, Chu W, Zhang H, Zou R and Xia D 2018 *Adv. Mater.* **30** 1707255
[5] Lu Z and Dahn J R 2002 *J. Electrochem. Soc.* **149** A815
[6] Croy J, Kang S-H, Balasubramanian M and Thackeray M 2011 *Electrochem. Commun.* **13** 1063
[7] Croy J R, Gallagher K G, Balasubramanian M, Long B R and Thackeray M M 2014 *J. Electrochem. Soc.* **161** A318
[8] Yu X, Lyu Y, Gu L, Wu H, Bak S M, Zhou Y, Amine K, Ehrlich S N, Li H and Nam K W 2014 *Adv. Energy Mater.* **4** 1300950
[9] Gent W E, Lim K, Liang Y, Li Q, Barnes T, Ahn S J, Stone K H, McIntire M, Hong J and Song J H 2017 *Nat. Commun.* **8** 1
[10] Armstrong A R, Holzapfel M, Novák P, Johnson C S, Kang S H, Thackeray M M and Bruce P G 2006 *J. Am. Chem. Soc.* **128** 8694
[11] Yin W, Grimaud A, Rousse G, Abakumov A M, Senyshyn A, Zhang L, Trabesinger S, Iadecola A, Foix D and Giaume D 2020 *Nat. Commun.* **11** 1
[12] Gallagher K G, Croy J R, Balasubramanian M, Bettge M, Abraham D P, Burrell A K and Thackeray M M 2013 *Electrochem. Commun.* **33** 96
[13] Xiao Z, Liu J, Fan G, Yu M, Liu J, Gou X, Yuan M and Cheng F 2020 *Mater. Chem. Front.* **4** 1689
[14] Ji X, Xia Q, Xu Y, Feng H, Wang P and Tan Q 2021 *J. Power Sources* **487** 229362
[15] Lan X, Xin Y, Wang L and Hu X 2018 *J. Nanopart. Res.* **20** 1
[16] Grenier J, Wattiaux A, Lagueyte N, Park J, Marquestaut E, Etourneau J and Pouchard M 1991 *Physica C* **173** 139
[17] Grenier J C, Pouchard M and Wattiaux A 1996 *Curr. Opin. Solid. ST. M.* **1** 233
[18] Grant P, Parkin S, Lee V, Engler E, Ramirez M, Vazquez J, Lim G, Jacowitz R and Greene R 1987 *Phys. Rev. Lett.* **58** 2482
[19] Labbe J and Bok J 1987 *Europhys. Lett.* **3** 1225

[20] Cardoso D, Šljukić B, Sousa N, Sequeira C, Figueiredo F and Santos D 2018 *Phys. Chem. Chem. Phys.* **20** 19045

[21] Grenier J, Wattiaux A, Doumerc J, Dordor P, Fournes L, Chaminade J and Pouchard M 1992 *J. Solid State Chem.* **96** 20

[22] Sanchez R, Torresi R, Rettori C, Oseroff S and Fisk Z 1995 *Electrochim. Acta* **40** 209

[23] Bhavaraju S, DiCarlo J, Yazdi I, Jacobson A, Feng H, Li Z and Hor P 1994 *Mater. Res. Bull.* **29** 735

[24] Pouchard M, Demourgues A, Weill F, Villesuzanne A, Wattiaux A and Grenier J 1994 *Adv. Mater. Res.* **1** 11

[25] Delville M H, Barbut D, Wattiaux A, Grenier J C and Etourneau J 2004 *J. Electrochem.Soc.***151** J69

[26] McKinnon W, Post M, Selwyn L, Pleizier G, Tarascon J, Barboux P, Greene L and Hull G 1988 *Phys. Rev. B* **38** 6543

[27] Kong G, Jones M O, Abell J S, Edwards P P, Lees S T, Gibbons K E, Gameson I and Aindow M 2001 *J. Mater. Res.* **11** 3309

[28] Zhang Z, Chen X, Zhang X, Lin H, Lin H, Zhou Y and Wang X 2013 *Catal. Commun.* **36** 20

[29] Wang X T, Li B, Kong D R, Zhang Z Y, Zhang X F, Deng Z P, Huo L H and Gao S 2022 *J. Alloys Compd.* **911** 165037

[30] Bruce P, Lisowska-Oleksiak A, Saidi M and Vincent C 1992 *Solid State Ionics* **57** 353

[31] Ning F, Li S, Xu B and Ouyang C 2014 *Solid State Ionics* **263** 46

[32] Li X, Su Z and Wang Y 2018 *J. Alloys Compd.* **735** 2182

[33] Wang C, Appleby A J and Little F E 2001 *J. Electroanal. Chem.* **497** 33

[34] Gordon I J, Grugeon S, Takenouti H, Tribollet B, Armand M, Davoisne C, Débart A and Laruelle S 2017 *Electrochim. Acta* **223** 63

[35] Sun X, Zhang X, Liu W, Wang K, Li C, Li Z and Ma Y 2017 *Electrochim. Acta* **235** 158

[36] Zhuang Q, Chen Z, Dong Q, Jiang Y, Huang L and Sun S 2006 *Chin. Sci. Bull.* **51** 1055

[37] Shigang L, Jiaoyang W, Shu Z, Jian G, Shaofei W and Hong Li 2015 *Energy Storage Sci. Technolo.* **4** 83